Resonant impulsive-stimulated Raman scattering on malachite green

J. Chesnoy and A. Mokhtari

Laboratoire d'Optique Quantique du Centre National de la Recherche Scientifique,
Ecole Polytechnique, 91128 Palaiseau Cédex, France
(Received 26 February 1988)

We have studied in the femtosecond regime the transient dynamics of dichroism (anisotropic absorption), birefringence, and frequency shift induced by an intense femtosecond pump beam in the dye malachite green in solution. Vibrational quantum beats were observed superimposed on the saturated absorption and dispersion signals and quantitatively explained in terms of impulsive-stimulated Raman scattering close to an electronic resonance. The selectivity for observation of the vibrations in the two electronic states is described for the different experimental schemes. We discuss the access to vibrational and electronic dynamics in both ground and excited electronic states and compare the possibilities to those of previous techniques.

INTRODUCTION

Various techniques exist that give access to the vibrational dynamics of molecules in the dense phase.[1] Among the available methods based on nonlinear optics, time-resolved coherent anti-Stokes Raman scattering (CARS) is a well-established technique to observe the vibrational phase decay.[2] The availability of femtosecond lasers has permitted several extensions of time-resolved vibrational spectroscopy. Impulsive-stimulated Raman scattering (ISRS) has been demonstrated.[3-5] Excitation and probing of low-frequency vibrational modes displayed real-time molecular oscillations. These oscillations appear as quantum beats of the diffraction efficiency of a transient-induced grating due to refractive-index modulations.

Recently, multiterahertz oscillations of saturated absorption were also observed in several dye molecules in solution.[6,7] These transmission quantum beats, of vibrational origin as well, were interpreted in the frame of a three-level system with two closely spaced levels in the upper electronic state.[8]

We reported in a preceding Letter different pump-probe measurements in the dye malachite green (MG) with femtosecond resolution.[9] Here we give a full account of this study with additional results. Induced dichroism, in its definition of anisotropic absorption, reproduces the beats obtained by Rosker and co-workers,[6,7] while induced birefringence displayed vibrational oscillations as well, but with a different origin. We show that the observed quantum beats can be explained in the framework of ISRS close to an electronic resonance so that absorption as well as dispersion beats are observable after a single beam excitation.[10] We show that vibrational excitation occurs in both ground and excited electronic states. In addition to the observation of vibrationally modulated induced absorption and dispersion, we performed a measurement of the frequency shift of the probe beam as well as its amplitude modulation, both of which display vibrational beats induced by the pump beam. We obtain theoretical expressions for the observed signal using sta-
tistical mechanics on the basis of a unidimensional vibronic system and discuss the molecular properties relevant to the observations.

I. EXPERIMENT AND RESULTS

A. Experiment

The experiment consists of a pump-probe measurement of light-induced dichroism, birefringence or frequency modulation of a probe beam after illumination of the sample by an intense pump light pulse (Fig. 1). The two pulses are obtained by the splitting of the output of a femtosecond dye laser [50–60 fs duration full width at half maximum (FWHM) at 50 MHz repetition rate] pumped by a frequency doubled continuously mode-locked Nd: yttrium aluminum garnet (YAG) laser.[11] The pump beam (15 mW average) is focused to a diameter around 15 μm in the $l = 160$-μm-thick sample jet containing malachite green in a 2×10^{-4} M solution. The 625-nm wavelength of the laser is close to the absorption maximum for MG in the three solvents that were investigated, water, ethylene glycol, and dimethylsulfoxide. The weak probe beam from the same laser is focused on the excited spot with a small angle. Its horizontal polarization is at 45° from the pump polarization in order to perform a polarization-sensitive detection.

As shown in Fig. 1, we first measured the transient dichroism and birefringence induced by the pump beam [cases (a) and (b) of Fig. 1]. The electric field of the pump beam can be written

$$\mathcal{E}(t) = E_0(t) \exp(i\omega_0 t) + \text{c.c.} \ ,$$

where $E_0(t)$ is the envelope. The probe pulse delayed by τ relative to the excitation has two equal components $\mathcal{E}_s(t - \tau)$ parallel $\mathcal{E}_{s\parallel}$ and perpendicular $\mathcal{E}_{s\perp}$ to the pump beam. After the sample, the probe field has experienced amplitude and phase variations, different for the parallel and perpendicular components. Its envelope is given by
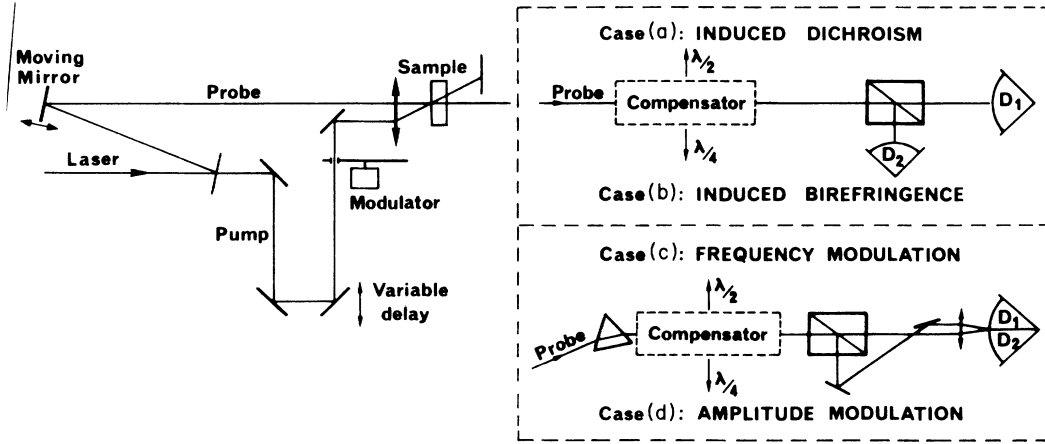
FIG. 1. The initial laser pulse is divided into two beams to perform the measurements in the pump-probe configuration. Nearly collinear pump and probe beams are focused in the sample, polarized 45° to each other. Four polarization-sensitive schemes are used, labeled (a)–(d). Beam energies given by detectors D_1 and D_2 are equalized and synchronous detection of $D_1 - D_2$ following modulation of the pump gives the experimental signals. In (a) the probe polarization rotation is measured, while tuning of the compensator to $\lambda/4$ gives access in (b) to the induced ellipticity. If a prism is used to disperse the probe beam, the frequency shift is measured by $D_1 - D_2$ in (c) (in fact, the difference in frequency shifts for two orthogonal polarizations). Tuning the compensator to $\lambda/4$ gives access in (d) to amplitude variations that can be visualized as delay time shifts. The moving mirror is oscillating to obtain the second derivative of the experimental signals (Ref. 16).

$$E_s(t-\tau,l)=E_{s\parallel}(t-\tau)e^{a_\parallel(t)+i\psi_\parallel(t)}+E_{s\perp}(t-\tau)e^{a_\perp(t)+i\psi_\perp(t)} .$$

(1)

The amplitude factors $a(t)$ originate from variations of the absorption coefficient $\Delta\Gamma_\parallel(t)$ and $\Delta\Gamma_\perp(t)$ and the phase factors $\psi(t)$ originate from variations of the refractive index $\Delta n_\parallel(t)$ and $\Delta n_\perp(t)$. In our first detection scheme [case (a) in Fig. 1], we measure the difference in energy $W_\parallel - W_\perp$ between parallel and perpendicular probe field components, versus the delay time τ, which is the standard method to measure the dichroism induced by the pump excitation:[12]

$$S_a(\tau)=\frac{W_\parallel - W_\perp}{W_\parallel}=-lR_\Gamma(t)\otimes C(t) ,$$

(2)

where $\otimes$ means a convolution with the intensity autocorrelation function

$$C(\tau)=\int I(t)I(t-\tau)dt \bigg/ \left[\int I(t)dt\right]^2$$

measured independently by harmonic generation. $R_\Gamma(t)$ is the response function of $\Delta\Gamma_\parallel - \Delta\Gamma_\perp$ to an instantaneous excitation. In our second detection scheme [case (b) in Fig. 1], a quarter wave plate is inserted after the sample at 45° to the probe polarization in order to give access to the time-resolved optical Kerr effect.[13] The measurement of the energy difference between the two directions parallel and perpendicular to the initial probe polarization gives the ellipticity induced in the probe pulse. Compared to the measurement of induced dichroism, this last measurement exchanges formally the roles of $a(t)$ and $\psi(t)$ in Eq. (1), and thus the response function $R_n(t)$ of the index of refraction ($\Delta n_\parallel - \Delta n_\perp$) is measured:

$$S_b(\tau)=\frac{2\pi l}{\lambda}R_n(t)\otimes C(t) .$$

(3)

These techniques, already exploited in previous studies,[12,13] possess high sensitivity due to the linear detection of the absorption or refractive-index variations and to the differential detection that limits the influence of probe intensity fluctuations. Detectivity of induced intensity variations within 10^{-5} is obtained with our system. In addition, with these techniques, absorption and dispersion perturbations are experimentally separated in contrast to the case of induced gratings measurements.[3–5] In our experimental configuration a Babinet-Soleil compensator is used after the sample tuned at $\lambda/2$ in order to get the induced dichroism signal $S_a(\tau)$ and at $\lambda/4$ to get the induced birefringence signal $S_b(\tau)$. They can be successively obtained without any other adjustment.

Two additional detection schemes were implemented to analyze spectral and amplitude perturbations of the probe beam as displayed in Fig. 1, cases (c) and (d). After the excitation, the probe pulse is sent into the sample with geometrical conditions identical to the above measurement. Then the probe pulse is spectrally dispersed by a prism on a dual photocell equilibrated to zero. In addition, the spectra of $\mathscr{E}_{s\parallel}$ and $\mathscr{E}_{s\perp}$ are expanded in opposite directions on the dual photocell. The difference in the energy received by the two detectors in thus proportional to the difference $\Delta\omega_\parallel - \Delta\omega_\perp$ between the frequency shifts experienced by the two probe polarizations. $\Delta\omega$ is the shift of the spectrum center of gravity ω_0:

$$S_c(\tau)=\Delta\omega(\tau)\propto \int_0^{\omega_0}E_s^*(\omega,l)E_s(\omega,l)d\omega$$
$$-\int_{\omega_0}^{\infty}E_s^*(\omega,l)E_s(\omega,l)d\omega .$$

(4)

To evaluate the origin of the measured signal, one can assume that $a(t) + i\psi(t)$ in Eq. (1) is small compared to 1 and varies slowly enough with time to be approximated by a second-order expansion in t. Then

$$E_s(\omega - \omega_0, \tau) = \int E_s(t - \tau) e^{-i\omega(t-\tau)} e^{a(t)+i\psi(t)} dt ,$$

$$E_s^*(\omega - \omega_0, \tau) E_s(\omega - \omega_0, \tau)$$

$$= E_s(\omega - \omega_0) E_s(\omega - \omega_0)[1 + 2a(\tau)]$$

$$+ E_s(\omega - \omega_0) \frac{d}{d\omega} E_s(\omega - \omega_0) \left[-2\frac{d\psi}{d\tau} \right] ,$$

(5)

where we have considered for simplicity that $E_s(t)$ and thus $E_s(\omega)$ are real and symmetric. The above calculation gives the result of the instantaneous frequency approximation[14] $[\Delta\omega(\tau) \simeq -d\psi/d\tau]$. Thus

$$S_c(\tau) \simeq \frac{-2\pi}{\lambda} l \frac{d}{dt} [R_n(t)] \otimes C(t) .$$

(6)

Breakdown of this approximation can be expected if terms higher than second order in time are not negligible in $a(t)$ and $\psi(t)$ or if the variation of $a(\tau)$ with the optical frequency ω is important.

In a last set of experiments a quarter wave plate is also inserted in the probe beam after the sample and before the frequency shift analysis [case (d) of Fig. 1]. The physical origin of the signal can be understood with the approximation leading to the above Eq. (6). Since the quarter wave plate exchanges the role of the phase $\psi(t)$ and amplitude $a(t)$, $S_d(\tau) \simeq -da(\tau)/d\tau$:

$$S_d(\tau) \simeq l \frac{d}{dt} [R_\Gamma(t)] \otimes C(t) .$$

(7)

Within these approximations, $S_d(\tau)$ measures the difference of the time shifts $\Delta\tau$ experienced by the two polarization components of the probe pulse:

$$\Delta\tau \simeq -\frac{da(\tau)}{d\tau} \frac{E(t=0)}{d^2E(t=0)/dt^2} .$$

(8)

Thus $S_d(\tau) \propto \Delta\tau$, if we neglect the delay given by the change of the index of refraction.

B. Results

Figure 2 represents four sets of experimental data obtained using the different detection schemes described above, in MG dissolved in water. In (a), we observe the decay of anisotropic saturated absorption (dichroism) induced by the pump beam, while in (b) we observe the induced birefringence (Kerr effect) due to induced saturated dispersion of the dye. Superimposed on the slowly varying decay, damped oscillations are displayed with a period close to 150 fs corresponding to a vibrational mode (~ 220 cm^{-1}) of MG. The decay $S_a(\tau)$ is the polarization analog of the beatings observed by Rosker et al.[6] in satured absorption, while $S_b(\tau)$ is the report of a vibrationally modulated time-resolved Kerr effect.

In Fig. 2(c), we observe that the probe beam frequency is shifted by the excitation and that vibrational oscillations are clearly displayed on this frequency shift. We
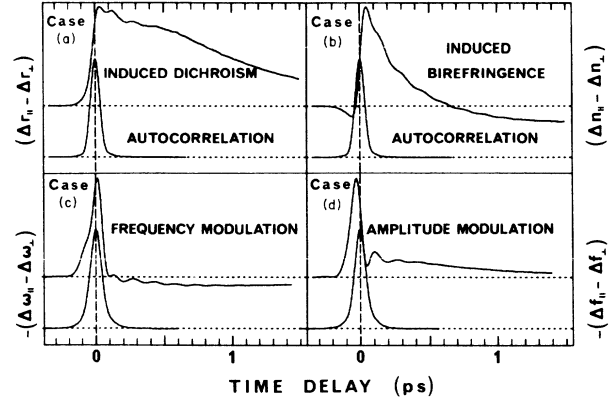
FIG. 2. For malachite green in water, the four experimental signals corresponding to the setup of Fig. 1 are displayed and indexed accordingly, cases (a)–(d). Induced dichroism (a) and birefringence (b) are obtained in successive runs, going from each other by tuning the compensator. Frequency modulation (c) and amplitude modulation (d) are likewise obtained successively by the frequency shift measurements. Small magnitude beatings are observed in each condition, superimposed on large backgrounds originating from saturated absorption and dispersion. At bottom, the experimental intensity autocorrelation function gives the time resolution and the zero time delay.

underline the sensitivity necessary to obtain this result since the magnitude of the frequency modulation is only several 10^{-2} cm^{-1} (compared to the 200 cm^{-1} laser bandwidth). Finally, the amplitude modulation $S_d(\tau)$ in Fig. 2(d) displays again vibrational oscillations superimposed on a slowly varying background. The sensitivity achieved gives access to a time delay shift of several tens of attoseconds as given by Eq. (8) (1 as $= 10^{-18}$ s).

In all these experiments, a sharp structure close to the zero time delay reveals the presence of the so-called coherent artefact due to the use of pulses from the same laser to pump and probe the sample.[15] The experimental curves will be exploited outside this perturbed range that is complicated by an additional thermal contribution.

The oscillatory experimental behavior is superimposed on a large slowly relaxing background, especially in the cases (a) and (b) of induced dichroism and birefringence. In order to perform a selective observation of the high-frequency variations of the experimental signals, we have developed a new technique described in detail elsewhere:[16] we modulate the time delay τ by using an oscillating mirror and detect the modulation of the probe beam by a phase-sensitive detection tuned to the harmonic frequency of the oscillation. For time delay oscillations short compared to the laser pulse duration, the signal $S^H(\tau)$ obtained by this technique is equal to the second derivative $d^2S(\tau)/d\tau^2$ of the direct signal $S(\tau)$. The same experimental procedure can be applied to obtain the intensity autocorrelation function $C^H(\tau)$. One can see that the measurements of induced dichroism (a) and birefringence (b) by this technique lead to
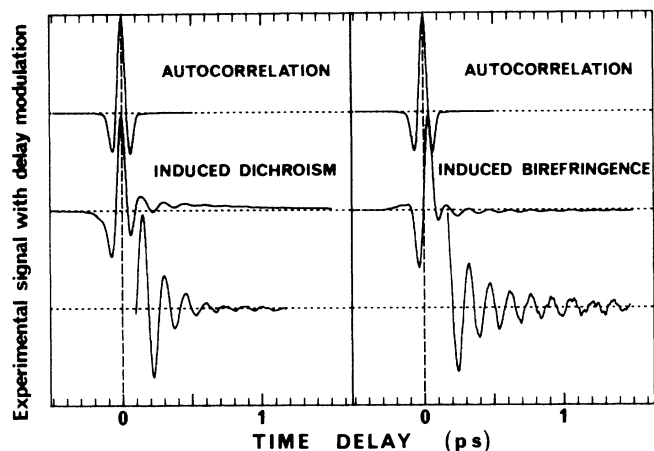
FIG. 3. Vibration of the time delay (using the moving mirror of Fig. 1) and synchronous detection of the signal at the harmonic of this vibration frequency permits us to measure the second derivative of the experimental signals (Ref. 16). This operation is displayed in (a) for induced dichroism and in (b) for induced birefringence, for the same conditions as in Figs. 2(a) and 2(b). The same procedure is applied to the intensity autocorrelation function (on top of the figure). At the bottom of the figure, the damped oscillations are now clearly extracted with improved signal to noise.

$$S_a^H(\tau) = -lR_\Gamma(\tau) \otimes C^H(\tau) ,$$

$$S_b^H(\tau) = \frac{2\pi l}{\lambda} R_n(\tau) \otimes C^H(\tau) ,$$

(9)

in close analogy with Eqs. (2) and (3). The apparatus function $C(\tau)$ is simply replaced by the function $C^H(\tau)$. Figure 3 displays the results obtained for induced absorption and dichroism in MG dissolved in water. The beating is extracted with a better signal to noise than in Figs. 2(a) and 2(b) as shown by the magnified scale at the bottom of Fig. 3.

The oscillatory decays were observed in three solvents, water, dimethylsulfoxide, and ethylene glycol with different viscosities and dielectric constants in order to test the influence of the solvent properties. In Fig. 4, the oscillating components of the induced dichroism (a) and birefringence (b) are displayed for the three solvents tested. In the case of frequency and amplitude modulations [cases (c) and (d)], the oscillations are detected with an acceptable signal-to-noise ratio on the direct signal. Thus a high-pass numerical filtering is sufficient to obtain the oscillating decay of Figs. 4(c) and 4(d) in water and ethylene glycol (the signal to noise was not acceptable in dimethylsulfoxide).

II. INTERPRETATION

Our experimental results clearly exhibit oscillations with a period close to 150 fs, which corresponds to the breathing mode of triphenylmethane[17] dyes observed at 225 cm^{-1} in MG.[18] To interpret our observations, we will refer to the impulse Raman excitation and probing.
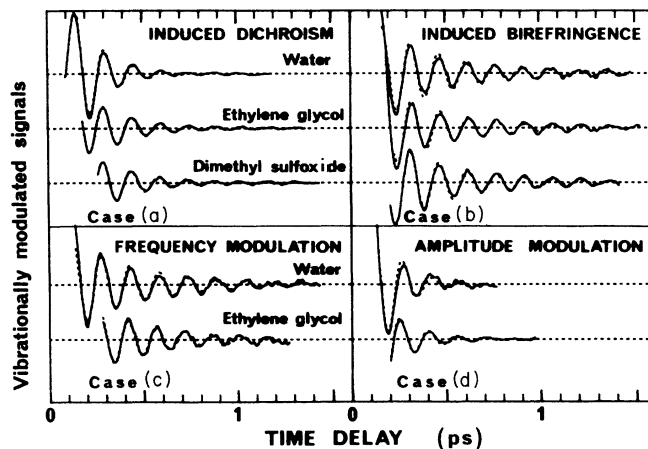
FIG. 4. The damped molecular oscillations are observed for malachite green in different solvents. The signals obtained for the different experimental configurations are indexed as cases (a)–(d) according to the notations of Figs. 1 and 2. The modulated part of the signal is obtained in (a) and (b) (induced dichroism and birefringence) by the technique illustrated in Fig. 3, and in cases (c) and (d) (frequency and amplitude modulation) the beating is selected by a high-pass numerical filter. In each experimental configuration the vibrational beatings are very similar in the different solvents (water, ethyleneglycol, dimethylsulfoxide). Quantitative comparison is made using a fit by a damped sinusoid superimposed as a dotted line on the data, with parameters given in Table I.

In contrast to a previous description of this effect,[10] we are in the resonant regime. This explains why we observe absorption as well as dispersion modulations in the medium; in addition, vibrations in both the ground and excited electronic states will be involved. We will develop a simple model to describe the origin of our observations. Finally, we will analyze what information can be extracted from our measurements concerning the dynamics inside the two electronic states.

A. Model

The pump laser pulse, with electric field $\mathscr{E}(t)$ $= E_0(t)e^{-i\omega_0 t + k_0 z} +$c.c., excites the molecular system as schematized in Fig. 5. The energy is plotted versus the vibrational coordinate Q of the breathing mode. The vibrational states in the ground electronic state S_0 (γ and γ', etc.) and in the excited state S_1 (β, β', etc.) have different equilibrium positions since the mode is optically active. We will restrict our calculation to this unidimensional model but will have then to consider the eventual additional effects of the relaxation of the other active vibrational modes in S_1 (going to S_1' in Fig. 4). The vibronic Hamiltonian H_0 is perturbed by the dipolar Hamiltonian of interaction with the pump light pulse $H_I(t) = -PE(t)$.

The time evolution of the system is described by the density matrix which satisfies the equation

$$\frac{d\rho}{dt} = \frac{1}{i\hbar}[H_0 + H_I(t), \rho(t)] + \frac{d}{dt}\rho_{\text{relax}} .$$ (10)

To obtain the vibrational quantum beats, we solve this equation by a perturbative approach.[19] At first order, coherences between states γ in S_0 and β in S_1 are excited,

$$\rho_{\gamma\beta}^1(t) = -\frac{i}{\hbar}P_{\gamma\beta}\rho_{\gamma\gamma}^0\int_{-\infty}^\infty R_{\gamma\beta}(t')E(t-t')dt' ,$$ (11)

where $P_{\gamma\beta}$ is the dipolar matrix element, $\rho_{\gamma\gamma}^0$ the equilibrium population in state γ, and $R_{\gamma\beta}(t)$ the response function of the $\rho_{\gamma\beta}^1$ elements equal in the Block approximation to

$$R_{\gamma\beta}(t) = e^{-(i\omega_{\gamma\beta}+1/T_{\gamma\beta})t} \quad \text{for } t > 0 .$$ (12)

At second order, populations and coherences are excited inside each electronic state:

Vibrational amplitude Q

FIG. 5. Schematization of the vibronic system describing the dye molecule excited by the laser at frequency ω_0 close to the electronic resonance. The unidimensional model with a single vibrational coordinate Q is accommodated to take into account the presence of several modes excited during the electronic transition. Their relaxation is accounted qualitatively by a shift of the unidimensional surface from S_1 to S_1'.

$$\rho_{\gamma\gamma'}^2(t) = -\frac{1}{\hbar^2}\int_{-\infty}^\infty dt''\int_{-\infty}^\infty dt'E(t-t'')E(t-t'-t'')R_{\gamma\gamma'}(t'')\sum_\beta P_{\gamma\beta}P_{\beta\gamma'}[\rho_{\gamma\gamma}^0 R_{\gamma\beta}(t') + \rho_{\gamma'\gamma'}^0 R_{\beta\gamma'}(t')] ,$$ (13)

$$\rho_{\beta\beta'}^2(t) = \frac{1}{\hbar^2}\int_{-\infty}^\infty dt''\int_{-\infty}^\infty dt'E(t-t'')E(t-t'-t'')R_{\beta\beta'}(t'')\sum_\gamma P_{\beta\gamma}P_{\gamma\beta'}\rho_{\gamma\gamma}^0[R_{\gamma\beta'}(t') + R_{\beta\gamma}(t')] ,$$ (14)

with $R_{\gamma\gamma'}$ and $R_{\beta\beta'}$ defined by the same Eq. (11).

The dephasing times $T_{\gamma\beta}$ between the two electronic states being short compared to the light pulse duration, the above expressions can be approximated by integration over t'. If we assume that the electronic dephasing times $T_{\gamma\beta}$ are the same for the different vibrational states ($T_{\gamma\beta} = T_e$),

$$\rho_{\gamma\gamma'}^2(t) = -\frac{1}{\hbar^2}\int_{-\infty}^\infty dt'E_0^2(t-t')\sum_\beta P_{\gamma\beta}P_{\beta\gamma'}\left[\frac{\rho_{\gamma\gamma}^0 R_{\gamma\gamma'}\left[t'-\frac{T_{\gamma\beta}^+}{2}\right]}{i(\omega_0+\omega_{\gamma\beta})+\frac{1}{T_e}} + \frac{\rho_{\gamma'\gamma'}^0 R_{\gamma\gamma'}\left[t'-\frac{T_{\gamma'\beta}^-}{2}\right]}{-i(\omega_0+\omega_{\gamma'\beta})+\frac{1}{T_e}}\right] ,$$ (15)

$$\rho_{\beta\beta'}^2(t) = -\frac{1}{\hbar^2}\int_{-\infty}^\infty dt'E_0^2(t-t')\sum_\gamma P_{\beta\gamma}P_{\gamma\beta'}\rho_{\gamma\gamma}^0\left[\frac{R_{\beta\beta'}\left[t'-\frac{T_{\gamma\beta'}^+}{2}\right]}{i(\omega_0+\omega_{\gamma\beta'})+\frac{1}{T_e}} + \frac{R_{\beta\beta'}\left[t'-\frac{T_{\gamma\beta}^-}{2}\right]}{-i(\omega_0+\omega_{\gamma\beta})+\frac{1}{T_e}}\right] ,$$ (16)

where $T_{\gamma\beta}^\pm = 1/[1/T_e \pm i(\omega_0+\omega_{\gamma\beta})]$.

Thus, second-order perturbation introduces vibronic population changes (for $\gamma = \gamma'$ and $\beta = \beta'$) and vibrational coherences in the ground electronic state Q_γ as well as in the excited state Q_β,

$$Q_\gamma(t) = \sum_{\gamma,\gamma'}\rho_{\gamma\gamma'}^2 q_{\gamma'\gamma}, \quad Q_\beta(t) = \sum_{\beta,\beta'}\rho_{\beta\beta'}^2 q_{\beta'\beta} ,$$ (17)

where $q_{\gamma\gamma'}(q_{\beta\beta'})$ are the vibrational matrix elements. For a harmonic oscillator with a mass m (m^γ or m^β) and a frequency ω (ω^γ or ω^β), only the response functions for $\gamma' = \gamma \pm 1$ and $\beta' = \beta \pm 1$ appear. Then

$$Q_\gamma(t) = 2\,\text{Re}\int_{-\infty}^\infty\frac{-dt'}{(2m^\gamma\omega^\gamma\hbar^2)^{1/2}}\sum_{\gamma,\beta}\sqrt{\gamma+1}P_{\gamma\beta}P_{\beta,\gamma+1}E_0^2(t-t')$$

$$\times\left[\frac{\rho_{\gamma\gamma}^0 R_{\gamma,\gamma+1}(t'-T_{\gamma\beta}^+)}{i(\omega_0+\omega_{\gamma\beta})+\frac{1}{T_e}} + \frac{\rho_{\gamma+1,\gamma+1}^0 R_{\gamma,\gamma+1}(t'-T_{\gamma+1,\beta}^-)}{-i(\omega_0+\omega_{\gamma+1,\beta})+\frac{1}{T_e}}\right] ,$$ (18)

$$Q_\beta(t) = 2\operatorname{Re}\int_{-\infty}^{\infty}\frac{dt'}{(2m^\beta\omega^\beta\hbar^2)^{1/2}}\sum_{\gamma,\beta}\sqrt{\beta+1}\,P_{\beta\gamma}P_{\gamma,\beta+1}E_0^2(t-t')\left[\frac{\rho_{\gamma\gamma}^0 R_{\beta,\beta+1}(t'-T_{\gamma,\beta+1}^+)}{i(\omega_0+\omega_{\gamma,\beta+1})+\dfrac{1}{T_e}}+\frac{\rho_{\gamma\gamma}^0 R_{\beta,\beta+1}(t'-T_{\gamma\beta}^-)}{-i(\omega_0+\omega_{\gamma\beta})+\dfrac{1}{T_e}}\right].$$

$$(19)$$

Vibrations are excited as a consequence of the presence of Fourier components at the oscillator frequency in the intensity profile $E_0^2(t)$. This impulsive Raman excitation occurs because the light spectrum contains at the same time the laser and Stokes frequencies. In the resonant regime, that we analyze here, impulsive Raman excitation occurs both in the ground and excited electronic states and the initial vibrational phases depend on the resonance mismatch.

With the single beam Raman excitation described here, the wave vectors of the vibrational excitations are simply

$$k^\gamma = \frac{\omega^\gamma n}{c}, \quad k^\beta = \frac{\omega^\beta n}{c}, \tag{20}$$

where n is the refractive index of the sample at the laser wavelength.

We consider now the probing of the excited volume by a pulse

$$E_s(t-\tau)e^{-i\omega_0(t-\tau)+k_s r}+\text{c.c.} ,$$

issued from the same beam as the pump pulse and focused with a relative delay τ after the pump. The polarization radiated by the probe pulse can be calculated by expansion of the density matrix up to the third order in the fields

$$P^3(t) = \frac{i}{\hbar^3}\sum_{\substack{\gamma,\beta\\\gamma',\beta'}}P_{\gamma\beta'}P_{\beta'\gamma'}P_{\gamma'\beta}P_{\beta\gamma}$$

$$\times\int_{-\infty}^{\infty}dt'''\int_{-\infty}^{\infty}dt''\int_{-\infty}^{\infty}dt'\,E_s(t-t'''-\tau)E_0(t-t'-t''')E_0(t-t'-t''-t''')$$

$$\times R_{\gamma\beta}(t''')\{R_{\gamma\gamma'}(t'')[\rho_{\gamma\gamma}^0 R_{\gamma\beta'}(t')+\rho_{\gamma'\gamma'}^0 R_{\beta\gamma'}(t')]$$

$$+R_{\beta\beta'}(t'')\rho_{\gamma'\gamma'}^0[R_{\gamma'\beta'}(t')+R_{\beta\gamma'}(t')]\} . \tag{21}$$

In this expression, we neglect the so-called coherent artefact that occurs from permutations of the electric fields. In Eq. (21), we recognize contributions to the polarization from vibrational levels in the ground electronic state and in the excited electronic state by $R_{\gamma\gamma'}(t')$ and $R_{\beta\beta'}(t')$, respectively.

Assuming an electronic dephasing time T_e faster than the pulse duration,

$$P^3(t) = \frac{i}{\hbar^3}\sum_{\substack{\gamma,\beta\\\gamma',\beta'}}E_s(t-\tau-T_{\gamma\beta}^+)e^{-i\omega_0(t-\tau)}\frac{P_{\gamma\beta'}P_{\beta'\gamma'}P_{\gamma'\beta}P_{\beta\gamma}}{i(\omega_0+\omega_{\gamma\beta})+\dfrac{1}{T_e}}$$

$$\times\int_{-\infty}^{\infty}dt'E_0^2(t-t')\left\{\left[\frac{\rho_{\gamma\gamma}^0 R_{\gamma\gamma'}\left[t'-\dfrac{T_{\gamma\beta'}^+}{2}\right]}{i(\omega_0+\omega_{\gamma\beta'})+\dfrac{1}{T_e}}+\frac{\rho_{\gamma'\gamma'}^0 R_{\gamma\gamma'}\left[t'-\dfrac{T_{\gamma'\beta'}^-}{2}\right]}{-i(\omega_0+\omega_{\gamma'\beta'})+\dfrac{1}{T_e}}\right]\right.$$

$$\left.+\left[\frac{\rho_{\gamma'\gamma'}^0 R_{\beta\beta'}\left[t'-\dfrac{T_{\gamma'\beta'}^+}{2}\right]}{i(\omega_0+\omega_{\gamma'\beta'})+\dfrac{1}{T_e}}+\frac{\rho_{\gamma'\gamma'}^0 R_{\beta\beta'}\left[t'-\dfrac{T_{\gamma'\beta}^-}{2}\right]}{-i(\omega_0+\omega_{\gamma'\beta})+\dfrac{1}{T_e}}\right]\right\} . \tag{22}$$

The perturbation of the probe beam is given by the propagation equations. In a frame moving with the pulse,

$$\frac{\partial E_p(t)}{\partial r} = \frac{ik}{2n^2}P^3(t)e^{i\Delta kr} , \tag{23}$$

k^γ or k^β being the wave vector of the vibrational excitation given by Eq. (20), the wave-vector mismatch is $\Delta k = k^\gamma(1-\cos\theta)$ [or $k^\beta(1-\cos\theta)$] where θ is the angle between pump and probe beams. For the oscillator frequency (~ 220 cm^{-1}) and experimental angle θ and sample length ($l = 160\ \mu$m), Δkr remains much smaller than

1. At the sample output,

$$E_p(t,l) \simeq E_p(t) + \frac{i\omega l}{2nc} P^3(t) \ . \tag{24}$$

Thus the probe pulse is perturbed by a phase and amplitude factor as assumed in Eq. (1),

$$a(t) = \mathrm{Re}\left[\frac{i\omega l}{2nc}\frac{P^3(t)}{E_p(t)} \right], \quad \psi(t) = \mathrm{Im}\left[\frac{i\omega l}{2nc}\frac{P^3(t)}{E_p(t)} \right] . \tag{25}$$

B. Discussion

The last equation shows that the radiated polarization perturbing the probe pulse is modulated by the response functions $R_{\gamma\gamma'}(t)$ and $R_{\beta\beta'}(t)$ of the vibrations in both ground and excited electronic states, in addition to the diagonal response functions $R_{\gamma\gamma}(t)$ and $R_{\beta\beta}(t)$ of the populations. The vibrational quantum beats observable are similar in principle to the previously reported quantum beats in transmission[20-22] and have different selection rules than in fluorescence detection.[19] The observation of the vibrational response functions $R_{\gamma\gamma'}(t)$ and $R_{\beta\beta'}(t)$ obtained by the density-matrix expansion at third order in the fields confirms that Eqs. (22)–(24) describe an ISRS quantum beat experiment. Far from resonance $P^3(t)$ is purely imaginary and only refractive-index modulations take place, related to the previously observed impulsive-stimulated Raman scattering where only the ground electronic state is involved. Closer to resonance, vibrations in both electronic states are involved, leading to joint absorption and dispersion modulation of the probe beam, as exhibited by our observations.

1. Vibrational oscillation and decay

A least-squares fit of the observed damped oscillation by a function

$$A \exp\left[-\frac{\tau}{T_2} \right] \cos(\omega_v \tau + \psi)$$

is plotted in Fig. 4. Table I gives the values obtained for ω_v and ψ. Small phase shifts due to the finite pulse duration are subtracted by deconvolution. Trials to fit the damped oscillations with a biexponential decay do not improve significantly the quality of the fit.

The acceptable fit by a monoexponential oscillating decay with ~ 150-fs period shows that only the breathing mode of MG at 220 cm^{-1} is involved. In fact, this mode is strongly Raman active and enhanced by the resonance.[17] It is isolated in frequency between weakly active higher modes[18] and overdamped torsional modes at lower frequencies.[23]

The observation of two different damping times T_2 shows that we observe vibrational dephasing in the ground electronic state S_0 as well as in the excited state S_1. The perturbation of the amplitude of the probe pulse (absorption effects) comes mainly from the high electronic state, while phase perturbations of the probe pulse (dispersion effects) originate from the ground electronic

TABLE I. Parameters obtained from the fit of the oscillating signals of Fig. 3 by a damped sinusoid: $\cos(\omega_v \tau + \psi) \exp(-\tau/T_2)$. A least-squares-fit method with multiple parameters is used. The phase shifts given by the experimental convolutions with the intensity autocorrelation function of the light pulse are subtracted in the tabulation of ψ. Cases (a)–(d) correspond to the experimental situations given in Fig. 1.

	Case (a) induced dichroism $-(\Delta\Gamma_\parallel - \Delta\Gamma_\perp)$			Case (b) induced birefringence $(\Delta n_\parallel - \Delta n_\perp)$			Case (c) frequency modulation $-(\Delta\omega_\parallel - \Delta\omega_\perp)$			Case (d) amplitude modulation $(\Delta f_\parallel - \Delta f_\perp)$		
	Oscillation period $\frac{2\pi}{\omega_v}$ (fs)	Damping constant T_2 (fs)	Phase ψ (deg)	Oscillation period $\frac{2\pi}{\omega_v}$ (fs)	Damping constant T_2 (fs)	Phase ψ (deg)	Oscillation period $\frac{2\pi}{\omega_v}$ (fs)	Damping constant T_2 (fs)	Phase ψ (deg)	Oscillation period $\frac{2\pi}{\omega_v}$ (fs)	Damping constant T_2 (fs)	Phase ψ (deg)
Water	152 (±3)	150 (±20)	8 (±20)	150 (±2)	330 (±30)	−40 (±20)	150 (±2)	350 (±30)	80 (±20)	153 (±4)	120 (±20)	135 (±20)
Ethylene glycol	151 (±2)	200 (±20)	10 (±20)	150 (±2)	330 (±30)	−60 (±20)	150 (±2)	350 (±30)	90 (±20)	151 (±2)	160 (±20)	145 (±20)
Dimethyl sulfoxide	148 (±2)	200 (±20)	3 (±20)	151 (±2)	340 (±30)	−30 (±20)						

state alone. As a matter of fact, the decay times for the induced birefringence [case (b)] and frequency modulation [case (d)] are comparable to the dephasing time derived from Raman spectroscopy [350 fs compared to ~ 400 fs (Ref. 18)], while the decay time for induced dichroism [case (a)] and amplitude modulation [case (d)] is much faster (around 140 fs). As indicated by Tang and co-workers[6,8] the modulation in saturated absorption gives access to the vibrational dephasing in the excited electronic state.

The nearly exponential oscillating decay indicates that the dephasing time T_2 and frequency ω_v are similar for the vibrational levels involved in a given electronic state. We must remark that a limited nonexponential deviation appears in all the experimental results, manifested by a small amplitude oscillation persisting after the complete damping of the fit. It remains difficult to demonstrate whether the vibrational dephasing is nonexponential or simply that the separation of vibrational dephasing in the ground and excited electronic state is not complete.

In all our experimental results, the fitted value of the vibrational period in the excited state (~ 154–155 fs) is very similar to its value in the ground electronic state (152–153 fs). The systematic shift of 2 fs lies within the experimental accuracy and would be compatible with a slightly less bonding excited electronic state.

An interesting point is the observation that the vibrational dynamics is very similar in the different solvents tested (having different molecular masses, viscosities, and dielectric constants, etc.) in contrast to the behavior of population relaxation very sensitive to solvent parameters.[23–25] This indicates that we observe vibrational dephasing of the isolated dye molecule or at least that the solvent does not intervene by its detailed structure. In addition, the solvent shifts of the absorption peak accompanying the different solvents have a negligible effect on the observed modulations, in agreement with their small amount (~ 10 nm) compared to the electronic resonance width (~ 50 nm).

2. Physical picture of resonant ISRS

A more quantitative feeling can be gained by additional approximations. For a harmonic oscillator damped by a quadratic perturbation potential, the response functions $R_{\gamma,\gamma+1}(t)$, or $R_{\beta,\beta+1}(t)$, are identical in all the vibrational states of a given electronic state:

$$R_{\gamma,\gamma+1}(t)=\exp(i\omega^\gamma t - t/T_2^\gamma) ,$$

and a corresponding equation holds for the β states. This approximation looks reasonable in our case since nearly exponential oscillating decays are observed. A simple expression for $Q_\gamma(t)$ and $Q_\beta(t)$ [Eqs. (18) and (19)] can be obtained if in addition we consider that the $\omega_{\beta\gamma}$ frequency can be replaced by an electronic frequency ω_e in the summation, that is justified by the Franck-Condon limitation of accessible vibrational states. Following an impulse excitation [$E_0^2(t)=\delta(t)$],

$$Q_\gamma(t)= \left[\frac{2}{m\omega^\gamma\hbar^3} \right]^{1/2} e^{-(t-T_e)/T_2^\gamma} \sum_{\gamma,\beta} \frac{-\sqrt{\gamma+1}P_{\gamma\beta}P_{\beta,\gamma+1}}{[(\omega_0-\omega_e)^2+1/T_e^2]^{1/2}} \{\rho_{\gamma\gamma}^0 \cos[\omega^\gamma(t-T_e)-\psi]+\rho_{\gamma+1,\gamma+1}^0 \cos[\omega^\gamma(t-T_e)+\psi]\} ,$$

(26)

with $\tan g\,\psi=(\omega_0-\omega_e)T_e$, and

$$Q_\beta(t)=\frac{2}{T_e} \left[\frac{2}{m\omega^\beta\hbar^3} \right]^{1/2} e^{-(t-T_e)/T_2^\beta}$$

$$\times \sum_{\gamma,\beta} \frac{\sqrt{\beta+1}P_{\beta\gamma}P_{\gamma\beta+1}}{(\omega_0-\omega_e)^2+1/T_e^2}\rho_{\gamma\gamma}^0 \cos[\omega^\beta(t-T_e)] ,$$

(27)

where we have also assumed that we are close enough to resonance so that $T_{\gamma\beta}^\pm=T_e$.

The physical picture of the resonant impulsive Raman excitation appears clearly: far from resonance $Q_\gamma(t)$ is excited with an amplitude proportional to $1/(\omega_0-\omega_e)$ and begins to oscillate following

$$\sin(\omega^\gamma t)\exp(-t/T_2^\gamma)$$

as in the case of a classical oscillator excited by a shock. $Q_\beta(t)$ in the high electronic state has a comparatively negligible amplitude [scaling as $1/(\omega_0-\omega_e)^2$]. When the resonance is approached, $Q_\gamma(t)$ and $Q_\beta(t)$ experience an enhancement of their excitation until $Q_\beta(t)$ in the high electronic state becomes excited with an amplitude comparable to $Q_\gamma(t)$ in the ground state. Excitation of $Q_\beta(t)$

in the high electronic state varies as the absorption profile and is important only in case of a strong vibronic coupling implying that Q_β and Q_γ have different equilibrium positions (otherwise $P_{\gamma\beta}P_{\beta\gamma+1}=0$). When the resonance is approached, $Q_\gamma(t)$ evolves from $\sin(\omega^\gamma t)$ to $\cos(\omega^\gamma t)$ at exact resonance. $Q_\beta(t)$ in the S_1 electronic state is phase locked to $\cos(\omega^\beta t)$ (within the electronic dephasing time T_e). The result of Eqs. (19) and (27) corresponds to the qualitative picture given in Refs. 18 and 26 (but not recognized there as Raman effect): excitation of vibrational populations in S_1 is accompanied by excitation of vibrational coherence and the oscillator undergoes oscillations from the side of the S_1 potential. Impulsive Raman excitation in the resonant case is characterized by communicating not only an initial velocity to the vibration but also an initial amplitude.

For the ground-state excitation, electronic population changes are not necessary and the amplitude $Q_\gamma(t)$ persists far from resonance following the dispersion profile of the electronic transition. At resonance, impulsive Raman excitation lead also to a nonzero initial amplitude of oscillation in S_0. We remark also that the finite value of the electronic dephasing time T_e imposes a time delay for the vibrational excitation close to resonance, while far from resonance no effect of electronic dephasing can be

detected any more since $T_{\gamma\beta}^{\pm} \simeq 0$.

In this classical picture, the probe beam experiences a change of absorption coefficient $\Delta\Gamma(t)$ and refractive index $\Delta n(t)$,

$$\Delta\Gamma(t) = \left| \frac{d\sigma_\gamma}{dq} Q_\gamma(t) + \frac{d\sigma_\beta}{dq} Q_\beta(t) \right| , \qquad (28)$$

$$\Delta n(t) = \frac{2\pi}{9n}(n^2+2)^2 \left| \frac{d\alpha_\gamma}{dq} Q_\gamma(t) + \frac{d\alpha_\beta}{dq} Q_\beta(t) \right| , \qquad (29)$$

where the real part of the polarizability α_γ (α_β) and absorption cross section σ_γ (σ_β) in each electronic state are derived versus the individual vibrational coordinate q. The observation of $Q_\gamma(t)$ in birefringence and frequency modulation [cases (b) and (c)] implies that $d\alpha_\beta/dq \ll d\alpha_\gamma/dq$, while observation of $Q_\beta(t)$ in dichroism and amplitude modulation [cases (a) and (d)] implies that $d\sigma_\gamma/dq \ll d\sigma_\beta/dq$.

The initial phases of the experimental damped oscillations can be compared to the above expressions, Eqs. (26) and (27). A phase ψ close to zero is observed for the induced absorption [case (a)] and compatible with its derivative [Eq. (8)] in amplitude modulation [case (d)] as shown in Table I. This means that the electronic dephasing time T_e is very short since it gives no detectable phase shift. Within the experimental phase precision of $\sim \pm 20°$, an upper limit for the electronic dephasing time T_e should be around 20 fs. Thus the electronic absorption band must have an important homogeneous character since a lower limit of 7 fs is given by the linewidth. A phase shift of 40° observed in induced birefringence [case (b)] and compatible with its derivative [Eq. (7)] in frequency modulation [case (c)] comes from the excitation of $Q_\gamma(t)$ close to the resonance but on the low-frequency side.

3. Information on the vibronic dynamics

We indicate above that an upper limit can be evaluated for the electronic dephasing time around 20 fs. In case of inhomogeneity of the electronic transition, not considered until here, we would expect to observe a superposition of experiments performed for different resonance conditions. Limited blurring of the observed oscillations would occur associated with a dispersion of the resonance conditions. Thus observation of ISRS quantum beats is weakly dependent on electronic inhomogeneity. In contrast, vibrational inhomogeneity (difference in vibrational frequency from molecule to molecule) would influence the observed vibrational decay.

Direct information is obtained about the dephasing dynamics of the breathing mode at 220 cm^{-1} in the ground electronic state S_0 as well as in the excited state S_1. The origin of the shortening of T_2 by more than a factor of 2 from S_0 to S_1 must be explained. Vibrational dephasing has two origins, energy relaxation T_1 and fluctuations of the oscillator frequency $\Delta\omega(t)$ (pure dephasing). In the fast modulation limit[27]

$$\frac{1}{T_2} = \frac{1}{2T_1} + \int_0^\infty \langle \Delta\omega(t)\Delta\omega(0) \rangle dt \qquad (30)$$

T_1 is due to the dissipation of energy towards other degrees of freedom.[28] Energy must be given to lower quantum states, which are in the present case solvent states or torsional modes strongly coupled to the solvent. As the vibrational dynamics that we observe is not solvent dependent, T_2 must be due to pure dephasing.

An anharmonic oscillator with Hamiltonian $H_0 = P^2/2m + \frac{1}{2}m\omega_0^2 Q^2 + (f/6)Q^3$ immersed in a bath suffers a time-dependent interaction Hamiltonian

$$V(t) = \frac{\partial V(t)}{\partial Q} Q + \frac{1}{2} \frac{\partial^2 V(t)}{\partial Q^2} Q^2$$

at second order in Q. Then[27]

$$\Delta\omega(t) = \left| \frac{-f}{2m^2\omega_0^2} \frac{\partial V}{\partial Q}(t) + \frac{1}{2m\omega_0} \frac{\partial^2 V}{\partial Q^2}(t) \right| . \qquad (31)$$

The bath is constituted by the other vibrational modes of the molecules and thus the derivatives of $V(t)$ versus Q in Eq. (31) are proportional to the crossed anharmonicities ($\partial^3 V/\partial Q^2 \partial Q_i$, $\partial^3 V/\partial Q \partial Q_i^2$, etc.). As a general rule, these crossed anharmonicities as well as the diagonal anharmonicity f are larger in the excited electronic state due to the smaller dissociation energy. Thus pure dephasing is expected to be faster in S_1 than in S_0 as we observe.

We observe selectively the oscillation of the breathing mode of MG as reported in previous experiments.[6,7] Other resonance enhanced Raman active modes are not observable since neither excitation nor probing is efficient outside the laser bandwidth. Triphenyl methane dyes look thus especially adapted to the unidimensional model developed above. Nevertheless, all the optically active modes of the MG molecule are excited. In our unidimensional model, the role of the other modes can be qualitatively taken into account by the shift of S_1 with time going to S_1' in Fig. 5 following the vibrational redistribution. Our experiment indicates that the transient oscillations are installed within a 100-fs delay.

4. Selective observations of vibrations in S_0 and S_1

We observe selectively the dynamics of Q_γ (in S_0) by dispersion experiments and the dynamics of Q_β (in S_1) by absorption experiments. The approximate expressions given by Eqs. (28) and (29) will allow us to interpret simply this feature.

Considering first the modulation of absorption and dispersion by the vibration of Q_γ in S_0, σ_γ and α_γ are determined by the linear susceptibility $X_a(\omega)$ of the dye molecule. Figure 6 gives the absorption curve of MG [$\sigma_a(\lambda)$] measured versus the wave number $1/\lambda$, and the associated dispersion curve $\alpha_a(\lambda)$ qualitatively plotted. A simple picture such as the free-electron gas model[29] indicates that the peak position λ_a is linearly dependent on the vibrational elongation Q_γ. If we consider that the perturbation of the spectrum by a change of Q_γ is limited to this shift, then

$$\frac{d\sigma_\gamma}{dq} = \frac{d\sigma_a}{d\lambda_0} \frac{d\lambda_a}{dq} , \quad \frac{d\alpha_\gamma}{dq} = \frac{d\alpha_a}{d\lambda_0} \frac{d\lambda_a}{dq} . \qquad (32)$$
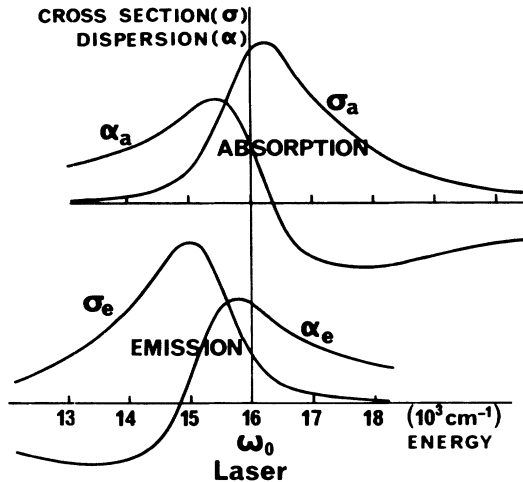
FIG. 6. Absorption and emission (fluorescence) spectrum of malachite green in water solution. The laser frequency ω_0 is close to the maximum of the absorption cross section σ_a and on the fast slope of the associated dispersion α_a, while the situation is opposite for the emission spectrum. The dispersion curve is calculated from the absorption measurement. The emission spectra are taken as the image by mirror symmetry of the absorption curve, with a fluorescence Stokes shift experimentally obtained by fluorescence up-conversion.

The derivative of the absorption cross section σ_a and dispersion α_a at the laser wavelength λ_0 indicate that, as we are close to the absorption peak (see Fig. 6), $d\sigma_a/d\lambda_0$ is very small and $d\alpha_a/d\lambda_0$ is maximum, so that we expect that absorption measurements will be insensitive on vibration in S_0, while dispersion experiments will have an enhanced sensitivity.

The same arguments can be developed for Q_β in S_1 but considering now the emission susceptibility $X_e(\omega)$ from S_1'. $X_e(\omega)$ is displaced by the emission Stokes shift as shown in Fig. 6. We can write

$$\frac{d\sigma_\beta}{dq} = \frac{d\sigma_e}{d\lambda_0}\frac{d\lambda_e}{dq}, \quad \frac{d\alpha_\beta}{dq} = \frac{d\alpha_e}{d\lambda_0}\frac{d\lambda_e}{dq}. \tag{33}$$

The laser wavelength is now on the wing of the emission curve, so that $d\alpha_\beta/dq$ is now close to zero while $\partial\sigma_\beta/dq$ is large. We are in the opposite configuration than for Q_γ. This picture explains simply why Q_γ in S_0 is observed in induced birefringence [case (b)] and frequency modulation [case (c)], while Q_β in S_1 is observed in induced absorption [case (a)] and amplitude modulation [case (d)].

If our interpretation is correct, scanning the laser wavelength off the electronic resonance would cause a loss of selectivity of absorption and dispersion experiments on the vibrational dynamics in the lower and upper electronic states.

5. Comparison with other experimental techniques

Previous ISRS experiments were performed with a grating configuration,[3,4] i.e., excitation with two beams

and probing by scattering on the dynamic grating. Though this configuration offers more polarization choices, detection of $|P^3(t)|^2$ (quadratic detection) is a handicap: intense amplified pulses are necessary and also data on absorption and dispersion changes cannot be experimentally separated. Recent work has permitted observation of stimulated Raman scattering induced by a single beam, by the induced Kerr effect,[30,31] or spectrum modulation.[32] The single beam excitation that we perform permits a very sensitive linear detection of the radiated polarization $P^3(t)$ with separation of absorption and dispersion dynamics, that is of prime importance close to an electronic resonance.

We also underline that, while the present observation of frequency and amplitude modulations is considered here simply as a verification of induced absorption and dispersion measurements, it offers in fact different possibilities. We have some indications that the derivative equations (7) and (8) are not strictly followed, which implies the presence of a contribution of frequency-dependent saturated absorption in the probe frequency shift (and of a similar contribution of frequency-dependent saturated dispersion in amplitude modulation). These contributions to phase modulation are usually neglected, though they may be of great importance in practice, for example, in order to understand short pulse formation in subpicosecond dye lasers.[33]

The time-resolved ISRS experiments were based on the same physical processes as time-resolved CARS.[1] Simply in the latter scheme, the vibrational frequency is excited by a beating between separate laser and Stokes pulses and can thus give access to selected high-frequency modes. Probing is obtained by analyzing a new spectral component at the Stokes or anti-Stokes frequency. We notice that our frequency modulation technique is the natural extension of this detection of new frequencies. Both ISRS and CARS techniques can be used to study vibrational dephasing. CARS has a clear advantage of selectivity and high-frequency coverage but gives only access to the envelope of the vibrational oscillation. The additional information of phase and period are given by ISRS. Also, by time-resolved CARS, a linear detection is delicate[34] and usually a quadratic detection is performed that gives no way to separate absorption and dispersion effects. The polarization-sensitive ISRS schemes demonstrated in this paper supply an efficient way to study the response function of vibrational oscillations excited resonantly.

CONCLUSION

We have described different experimental manifestations of impulsive-stimulated Raman scattering in the resonant regime. We report the clear identification of Raman beats induced by a single beam ISRS excitation. The polarization-sensitive linear coherent detection that we use gives access separately to phase, amplitude as well as frequency modulations of a laser beam by ISRS. Our observations show the main trends of resonant ISRS such as the appearance of an absorptive effect in addition to pure dispersive manifestations. By an expansion of the

density matrix up to third order in the fields, we have described the observation of real-time vibrational oscillations in both ground and excited electronic states close to an electronic resonance, for a time-resolved saturated absorption or dispersion experiment. In particular, we show explicitly that the absorption quantum beats reported in Refs. 6 and 7 can be interpreted in terms of impulsive-stimulated Raman scattering (mainly in the S_1 electronic state) in a theoretical framework common with the description of the induced Kerr quantum beats reported here (originating mainly from the S_0 electronic state). A simple model used for a vibronic system allows

discussion of the physical parameters responsible for the observed experimental data. Vibrational dephasing is discussed as well as the electronic dynamics.

Tunable femtosecond pulses would lead to extremely promising spectroscopic applications of this effect such as the observation of the deformation of the electronic spectrum[35,36] accompanying a vibrational oscillation. In addition, the scheme that we demonstrate to analyze frequency modulations of a probe pulse opens a new experimental access to the variation with frequency of time-dependent nonlinear phenomena, a field that remains to be prospected theoretically.

[1]*Time-Resolved Vibrational Spectroscopy*, edited by A. Laubereau and M. Stockburger (Springer-Verlag, Berlin, 1985).

[2]A. Laubereau and W. Kaiser, Rev. Mod. Phys. 50, 607 (1978).

[3]M. M. Robinson, Y. X. Yan, E. B. Gamble, L. R. Williams, J. S. Meth, and K. A. Nelson, Chem. Phys. Lett. 112, 491 (1984).

[4]S. De Silvestri, J. G. Fujimoto, E. P. Ippen, E. B. Gamble, L. R. Williams, and K. A. Nelson, Chem. Phys. Lett. 116, 146 (1985).

[5]M. R. Farrar, L. R. Williams, Y. X. Yan, L. T. Cheng, and K. A. Nelson, in *Ultrafast Phenomena V*, edited by G. E. Fleming and A. E. Siegman (Springer-Verlag, Berlin, 1986).

[6]M. J. Rosker, F. W. Wise, and C. L. Tang, Phys. Rev. Lett. 57, 321 (1986).

[7]F. W. Wise, M. J. Rosker, and C. L. Tang, J. Chem. Phys. 86, 2827 (1987).

[8]M. Mitsunaga and C. L. Tang, Phys. Rev. A 35, 1720 (1987).

[9]A. Mokhtari and J. Chesnoy, Europhys. Lett. 5, 523 (1988).

[10]Y. X. Yan, E. B. Gamble, and K. A. Nelson, J. Chem. Phys. 83, 5391 (1985).

[11]J. Chesnoy and L. Fini, Opt. Lett. 11, 635 (1986).

[12]A. Migus, A. Antonetti, J. Etchepare, D. Hulin, and A. Orszag, J. Opt. Soc. Am. B 2, 584 (1985).

[13]E. P. Ippen and C. V. Shank, Appl. Phys. Lett. 26, 921 (1975).

[14]F. Shimizu, Phys. Rev. Lett. 19, 1097 (1967).

[15]E. P. Ippen and C. V. Shank, in *Ultrashort Light Pulses*, edited by S. L. Shapiro (Springer-Verlag, Berlin, 1984).

[16]J. Chesnoy and A. Mokhtari, Rev. Phys. Appl. 22, 1743 (1987).

[17]L. Angeloni, G. Smulevitch, and P. M. Marzocchi, J. Raman Spectrosc. 8, 305 (1979).

[18]K. A. Nelson and L. R. Williams, Phys. Rev. Lett. 58, 745 (1987); J. M. Y. Ha, H. J. Maris, W. M. Risen, J. J. Tauc, C. Thomsen, and C. Vardeny, *ibid.* 57, 3302 (1986).

[19]S. Haroche, in *High-Resolution Laser Spectroscopy*, Vol. 13 of *Topics in Applied Physics*, edited by K. Shimoda (Springer-Verlag, Berlin, 1976).

[20]T. W. Ducas, M. G. Littman, and M. L. Zimmerman, Phys. Rev. Lett. 35, 1752 (1975).

[21]W. Lange and J. Mlynek, Phys. Rev. Lett. 40, 1373 (1978).

[22]J. M. Mlynek and W. Lange, Opt. Commun. 30, 337 (1979).

[23]A. Mokhtari, L. Fini, and J. Chesnoy, J. Chem. Phys. 87, 3429 (1987).

[24]V. Sundstrom and T. Gillbro, J. Chem. Phys. 81, 3463 (1984).

[25]D. Ben Amotz and C. B. Harris, J. Chem. Phys. 86, 4856 (1987).

[26]S. Ruhman, A. G. Joly, B. Kohler, L. R. Williams, and K. A. Nelson, Rev. Phys. Appl. 22, 1717 (1987).

[27]D. W. Oxtoby, Adv. Chem. Phys. 40, 1 (1979).

[28]J. Chesnoy and G. M. Gale, Ann. Phys. (Paris) 9, 893 (1984).

[29]H. Kuhn, in *Progress in the Chemistry of Organic Natural Products*, edited by D. L. Zechmeister (Springer, Vienna, 1958).

[30]S. Ruhman, A. G. Joly, and K. A. Nelson, IEEE J. Quantum Electron. QE-24, 460 (1988).

[31]D. M. Morrow, W. T. Lotshaw, and G. A. Kenney Wallace, IEEE J. Quantum Electron. QE-24, 443 (1988).

[32]S. Ruhman, A. G. Joly, and K. A. Nelson, J. Chem. Phys. 86, 6563 (1987).

[33]O. E. Martinez, R. L. Fork, and J. P. Gordon, Opt. Lett. 9, 156 (1984).

[34]M. Van Exter and A. Lagendijk, Opt. Commun. 56, 191 (1985).

[35]C. H. Brito Cruz, R. L. Fork, W. H. Knox, and C. V. Shank, Chem. Phys. Lett. 132, 341 (1986).

[36]L. R. Williams and K. A. Nelson, J. Chem. Phys. 87, 7346 (1987).